The Solution Structure of a Monocyclic Analogue of Endothelin [1,15 Aba]-ET-1, Determined by ^{1}H NMR Spectroscopy

Murray Coles, Sharon L. A. Munro, and David J. Craik*

School of Pharmaceutical Chemistry, Victorian College of Pharmacy, Monash University, 381 Royal Parade, Parkville, Victoria, Australia 3052

Received September 27, 1993•

The structure of [1,15 Aba]-ET-1 has been determined in aqueous acetonitrile solution (10% acetonitrile, 1.5% acetic acid). [1,15 Aba]-ET-1 is an analogue of endothelin (ET-1) in which the disulfide bridge linking residues 1 and 15 has been removed by replacement of the cysteine residues with the mimicking group α-aminobutyric acid (Aba). The structure has been determined by ^{1}H NMR spectroscopy and simulated annealing calculations based on NOE constraints, $^3J_{HN-H\alpha}$ scalar coupling constants, and amide-proton-exchange rates. Distance information was extracted from 2D NOESY spectra using full-relaxation matrix techniques (utilizing the program DISCON). The structure can be described in terms of three defined segments: a type I β-turn over residues 5–8, a helix over residues 9–16, and a structured C-terminus over residues 17–21. The data indicate that some conformational averaging occurs throughout the peptide, particularly for residues 1–4 in the N-terminus, where no preferred conformation is present. The structure is compared with those previously reported for native ET-1. In general, removal of the disulfide bridge does not cause a major structural change in the helical and turn regions of the sequence, but increased structural disorder is noted at the N-terminus. The implications of the monocyclic analogue's conformation for the pharmacological activity and the ET_A/ET_B selectivity of the endothelin family of peptides and analogues are described. The N-terminus is proposed to be a key structural region for differentiation of binding activity at the ET_A and ET_B receptor sites.

Introduction

Endothelin (ET-1) is an endogenous peptide hormone which has attracted considerable attention due to its potent vasoconstrictor activity and extremely long-lasting pressor effect. Originally isolated from cultured porcine aortic endothelial cells by Yanagisawa et al.,[1] it has since been found to be the first member of a family of closely related peptides, all members of which consist of 21 amino acid residues and are bicyclic with two disulfide bridges (linking residues 1–15 and 3–11). The sequences of ET-1 and two further endothelins, ET-2 and ET-3, are encoded in the human genome[2] and also in the genomes of other mammals. For example, ET-1 and ET-2 have been found in the dog[3,4] and ET-3 in the rat[5] and the rabbit.[6] In addition, the family includes a fourth mammalian peptide, vasoactive intestinal contractor (VIC, also called endothelin-β), identified in the genome of the mouse[7] and several snake toxins, including the sarafotoxins (SRTX S6) isolated from the burrowing asp *Atractaspis engaddensis*.[8]

Two distinct receptor subtypes have been identified for the endothelins, ET_A[9] and ET_B.[10] The activity of members of the endothelin family at these two receptors is different, with ET-1 and ET-2 being selective agonists at ET_A,[9,11] whereas all members of the endothelin family are approximately equipotent at ET_B.[12] ET_A is distributed predominantly in cardiovascular tissue and ET_B in a wider range of tissues, including the kidneys and cerebellum.[13,14]

The conservation of the disulfide bridges in all members of the endothelin family has led to investigations of their importance in the expression of biological activity. Monocyclic and linear analogues of ET-1, where the cysteine residues have been replaced by other residues, have been particularly useful for this purpose. Such peptides vary markedly in terms of their biological activity, receptor binding, and ET_A/ET_B selectivity.[12,15-18] To date, however, the effect of such disulfide replacements on the solution conformation of the resulting peptides relative to that of native ET-1 is largely unknown. This report describes the solution structure of [1,15 Aba]-ET-1, an analogue of ET-1 in which the cysteine residues have been replaced by α-aminobutyric acid, Aba (Figure 1). This amino acid is commonly used as an isosteric replacement for cysteine.[19] The structure of this monocyclic ET-1 analogue has been determined in aqueous solution (10% acetonitrile, 1.5% acetic acid) by 2D ^{1}H NMR spectroscopy and simulated annealing calculations.

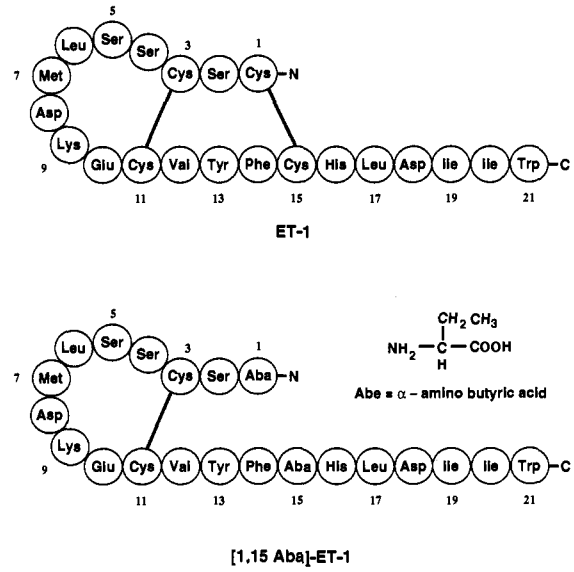

Figure 1. Amino acid sequences and disulfide connectivities of ET-1 and [1,15 Aba]-ET-1. The molecular structure of the cysteine-replacing amino acid, α-aminobutyric acid (Aba), is also shown.

* Author for correspondence.
• Abstract published in *Advance ACS Abstracts*, January 15, 1994.

0022-2623/94/1837-0656$04.50/0

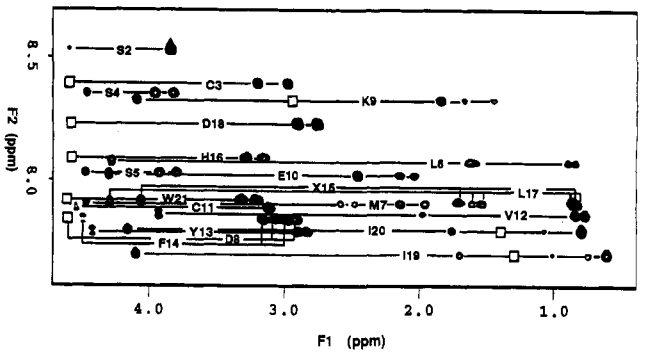

Figure 2. TOCSY spectrum of [1,15 Aba]-ET-1 (600 MHz, 298 K, 1.3 mM) showing connectivities between the NH protons and the side-chain spin systems. Residue numbers are indicated. Open squares indicate where cross peaks were observed but are not visible at this plot level.

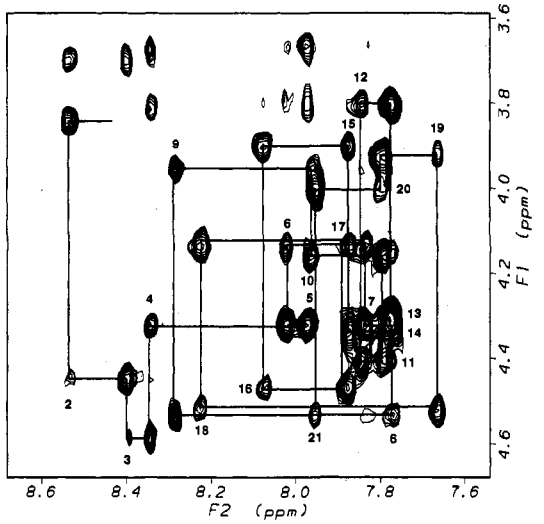

Figure 3. Sequential connectivities observed for [1,15 Aba]-ET-1 in the H_α–H_N fingerprint region of the 200-ms NOESY spectrum for a 1.3 mM solution at 293 K. Intraresidue cross peaks are indicated by residue number.

Results

Assignment of the NMR spectrum of [1,15 Aba]-ET-1 was carried out using the sequential assignment method of Wüthrich[20] in which peaks are first assigned to an amino acid type and then their sequential position is assigned by determining NOESY connectivities between adjacent residues. For [1,15 Aba]-ET-1, the side-chain spin system of each amino acid residue was identified mainly from amide-proton connectivities in the 2D TOCSY spectrum in H_2O (Figure 2). Ambiguities were resolved by reference to the DQF-COSY spectrum. Early in the process, the side chains of the three serine residues (Ser2, Ser4, and Ser5) were readily identified, and examination of the NOESY spectrum led to the assignment of a series of $d_{\alpha N}(i, i + 1)$ connectivities spanning residues 1–6. Identification of the unique side-chain spin systems of Lys9 and Val12 similarly led to the assignment of residues 8–13, as Glu10 was distinguished from the similar spin system of Met7, and Tyr13 from Phe14. Connectivities in 2D NOESY spectra between aromatic and H resonances in His16 and Trp21 identified these residues, leading to the assignment of residues 15–21, thus completing the assignments. The back-bone sequential assignments are summarized in Figure 3, which shows the connectivities observed for [1,15 Aba]-ET-1 in the NOESY spectrum at 293 K (mixing time = 200 ms). The chemical shifts of all proton resonances at this temperature are given in Table 1.

Table 1. Chemical Shifts (ppm) of [1,15 Aba]-ET-1 at 293 K

residue	NH	Hα	Hβ	others
Aba1		3.93	1.83	γCH_3 0.94
Ser2	8.63	4.54	3.79	
Cys3	8.49	4.68	3.14, 2.93	
Ser4	8.43	4.41	3.91, 3.77	
Ser5	8.06	4.42	3.89, 3.76	
Leu6	8.11	4.23	1.57	γCH_2 1.66; δCH_3 0.99, 0.93
Met7	7.93	4.42	2.09, 1.90	γCH_2 2.53, 2.42; ϵCH_3 2.01
Asp8	7.86	4.63	3.02, 2.86	
Lys9	8.42	4.17	1.79	γCH_2 1.40, 1.36; δCH_2 1.60; ϵCH_2 2.93; Nh_2 7.46
Glu10	8.38	4.05	2.10, 1.98	γCH_2 2.42, 2.32
Cys11	7.88	4.50	3.05, 3.03	
Val12	7.94	4.90	1.92	γCH_3 0.79, 0.70
Tyr13	7.87	4.39	2.86, 2.79	2,6H 6.87; 3,5H 6.66
Phe14	7.87	4.43	3.09, 2.92	2,6H 7.18; 3,5H 7.27; 4H 7.21
Aba15	7.97	3.99	1.66	γCH_3 0.84
His16	8.17	4.56	3.22, 3.11	2H 8.70; 4H 7.20
Leu17	7.97	4.23	1.56	γCH_2 1.47; δCH_3 0.80, 0.76
Asp18	8.32	4.63	2.86, 2.71	
Ile19	7.77	4.01	1.63	γCH_2 1.29, 0.96; γCH_3 0.51; δCH_3 0.69
Ile20	7.89	4.10	1.71	γCH_2 1.32, 1.04; γCH_3 0.74; δCH_3 0.72
Trp21	8.05	4.63	3.28, 3.16	2H 71.6; 4H 7.56; 5H 7.05; 6H 7.13; 7H 7.29

Stereospecific assignments were made for the prochiral H resonances of 5 of the 11 AMX spin systems. This was completed from considerations of cross-peak patterns in the 2D TOCSY spectra in deuterated solvent in conjunction with peak intensities in NOESY experiments.[21] In residues where stereospecific assignment was obtained, the χ^1 torsion angle of the predominant rotamer was also determined. In cases where stereospecific assignment could not be obtained, either the prochiral Hβ resonances were very similar in chemical shift or the data could not be interpreted unambiguously, presumably due to rotation about the χ^1 torsion angle. Stereospecific assignment was also possible for the γ-methylene protons of Ile19 and Ile20, and in these cases, the predominant rotamer about χ^1 or χ^2 was also determined.

A summary of sequential and long-range NOE connectivities is presented in Figure 4. Also indicated are $^3J_{HN-H\alpha}$ scalar coupling constants measured as greater than 8.0 Hz or less than 6.0 Hz and amide protons identified as exchanging slowly with solvent. A qualitative analysis of the data provides evidence of elements of secondary structure in several regions of the peptide, as described below.

A number of $d_{\alpha N}(i, i + 3)$, $d_{\alpha N}(i, i + 4)$, and $d_{\alpha\beta}(i, i + 3)$ connectivities are observed for residues 9–16 and are typical of a helical structure. Strong $d_{NN}(i, i + 1)$ connectivities, also indicative of helix, were observed in this region. However, with the exception of Lys9 HN–Glu10 HN and Glu10 HN–Cys11 HN, extensive shift coincidence of the amide-proton resonances involved made quantitation of these cross peaks difficult due to their close proximity to the diagonal. Further support for a helical structure comes from the series of slowly exchanging amide protons from residues 12–16, suggesting the formation of intramolecular hydrogen bonds.

A strong $d_{NN}(i, i + 1)$ cross peak between residues Leu6 and Met7, together with a number of weak connectivities between residues Ser5 and Asp8 and $^3J_{HN-H\alpha}$ coupling

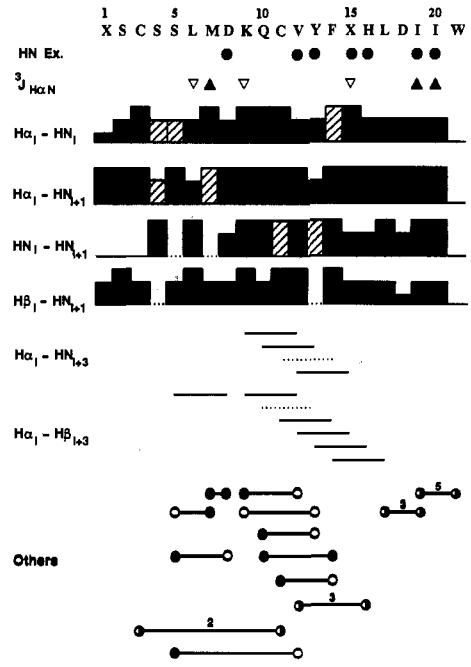

Figure 4. Summary of the observed NOE connectivities for [1,15 Aba]-ET-1 in the 200-ms NOESY spectrum at 293 K. The observed NOEs are classified into four levels as quantified by the height of the bars. Hatched bars and dashed lines indicate where quantification of the intensities was not possible due to spectral overlap. Medium and long connectivities are also marked. Filled and open circles represent connectivities between backbone and side chains, respectively. The number of occurrences of each type is indicated above the bar. $^3J_{H\alpha N}$ scalar coupling constants measured as greater than 8.0 Hz (▲) or less than 6.0 Hz (▽) are indicated, as are amide protons identified as exchanging slowly with solvent (●).

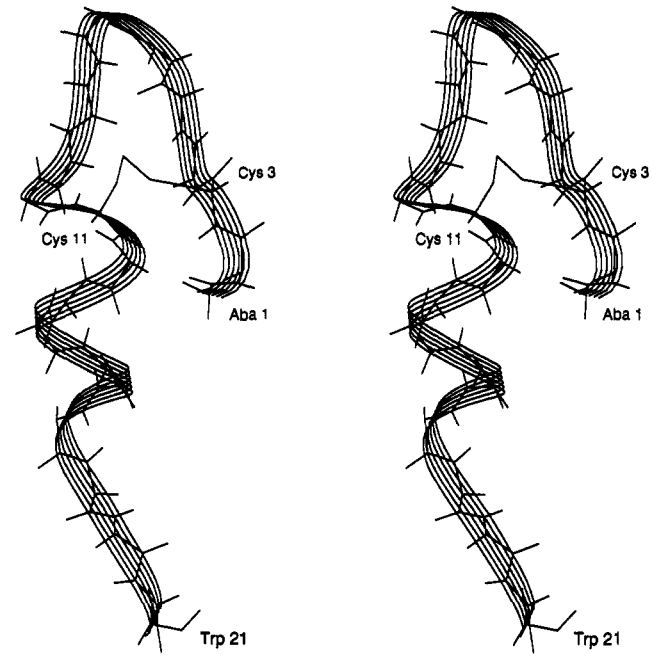

Figure 5. Stereoview of the lowest-energy structure for [1,15 Aba]-ET-1. Back-bone atoms are shown for all residues, as are heavy atoms in the disulfide bridge. Side chains are not shown for clarity.

constants for Leu6 and Met7 of <6.0 and >8.0 Hz, respectively, is indicative of a turn structure about residues 5–8. This is supported by the observation of a slowly exchanging amide proton of Asp8.

The large number of connectivities observed in the C-terminal region involving residues 17–21, especially $d_{NN}(i, i+1)$, and numerous $d(i, i+2)$ cross peaks indicate that this region of the peptide is also structured. The precise nature of the structure, however, is not apparent from a qualitative analysis of the NOEs.

Over the complete peptide sequence, only three connectivities have a span of more than four residues: two involve Ser5 and Val12 and another involves the cysteine residues 3 and 11, which form the disulfide bridge. These long-range NOEs assist in defining the spatial relationships between the local structured elements noted above. Given the relatively small size of the peptide, the existence of any long-range NOEs provides good support for the presence of a well-defined global fold.

The qualitative analysis of NOE and exchange data described above strongly suggests that [1,15 Aba]-ET-1 adopts a well-defined conformation in solution. To more precisely determine the nature of this conformation, a series of simulated annealing structure calculations was performed using the experimental NOE data as distance constraints.

Structure Calculations

Quantitative analysis of the NOE intensities yielded 144 sequential and 31 medium- and long-range distance constraints from experiments at 293 K and an additional three sequential and two medium-range constraints from experiments at 288 K. Six torsion angle constraints were included on the basis of the observations given in Figure 4. The ϕ angles of Leu6, Lys9, and Aba15 were constrained to $-60° \pm 30°$, and those of Met7, Ile19, and Ile20 were constrained to $-120° \pm 50°$. Three further χ_1 or χ_2 torsions were included for non-AMX residues which had been stereospecifically assigned (Val12 $\chi_1 = 60°$, Ile19,Ile20 $\chi_2 = -60°$). The χ_1 angles of AMX residues were not constrained in the simulation.

The structure calculation protocol outlined in the Experimental Section yielded sets of 40 structures for [1,-15 Aba]-ET-1. Preliminary sets of structures were calculated without H-bond constraints in order to determine possible H-bond acceptors for the slowly exchanging amide protons indicated in Figure 4. The average distance from each slowly exchanging amide proton to possible H-bond acceptors was measured to determine the likely H-bond acceptor. Three hydrogen bonds are suggested, namely Asp8 HN → Ser5 CO, Tyr13 HN → Lys9 CO, and His16 HN → Val12 CO, and these were included as constraints in the final structure calculations. No acceptor was unambiguously suggested by this analysis for the two slowly exchanging amide protons in the C-terminal region of the peptide, Ile19 HN and Ile20 HN.

The final set of 40 structures was calculated after the inclusion of dihedral and H-bond constraints. Ten of these structures were rejected on the basis of violation of the experimental constraints, leaving a set of 30 accepted structures. The root mean square deviation of the structures on the basis of back-bone atoms, calculated as the average of all possible pairwise comparisons, was 3.2 Å. A stereoview of the back-bone atoms of the lowest-energy structure calculated for [1,15 Aba]-ET-1 is shown in Figure 5.

Although the rms deviation of the global superimposition is high, the level of agreement obtained between structures is demonstrated if the peptide is considered as consisting of several segments. Two recognizable elements of sec-

Table 2. Average Back-Bone Torsion Angles[a] ϕ and ψ for [1,15 Aba]-ET-1

residue no.	ϕ	ψ	residue no.	ϕ	ψ
1		153	12	−126	−45
2	−72	123	13	−72	−10
3	−74	172	14	−88	−22
4	−60	25	15	−102	−35
5	−174	172	16	−110	66
6	−57 (−60)[b]	−17 (−30)	17	−135	33
7	−81 (−90)	−14 (0)	18	77	94
8	−126	171	19	−143	105
9	−131	−45	20	−107	34
10	−76	14	21	−46	
11	−121	−1			

[a] Angles in degrees. [b] Values in parentheses are standard torsion angles for a type I β-turn.[23]

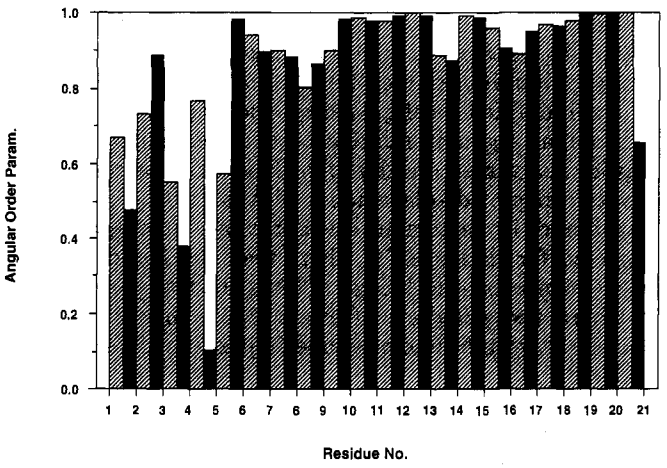

Figure 6. Angular order parameters for back-bone torsion angles of the 30 structures calculated for [1,15 Aba]-ET-1. For each residue, ϕ and ψ are shown as filled and hatched bars, respectively.

ondary structure have been identified, namely a β-turn at residues 5–8 and a helix for residues 9–16. In addition, a well-defined region also exists for the C-terminus (residues 17–21). The calculated structure is well defined within these individual segments; however, the relationship of the segments to each other varies considerably, leading to poor superimposition of the molecule as a whole. A fourth segment comprising the N-terminus (residues 1–4) does not show a preferred conformation.

The average back-bone torsion angles for the calculated structures are shown in Table 2. Angular order parameters[22] were calculated to provide a measure of the variation of individual torsion angles between structures. Values of this parameter approach unity where the angles are in complete agreement, falling to zero where they are randomly distributed. Figure 6 shows angular order parameters for the angles of each residue for the set of 30 calculated structures. Values of this parameter are generally high within the segments mentioned above. Slightly lower values for angles at the borders of the regions indicate a higher degree of local variation, suggesting these residues act as hinges for segmental motion. The disordered nature of the N-terminal segment (residues 1–4) is also clearly demonstrated.

Given the nature of the structure, further analysis was done separately on the individual segments. These are referred to as the β-turn, helix, C-terminus, and N-terminus segments. The nature of the structure calculated in each segment is discussed in detail in the following sections.

β-Turn. The structure of the segment comprising residues 5–8 can be described as a type I β-turn stabilized

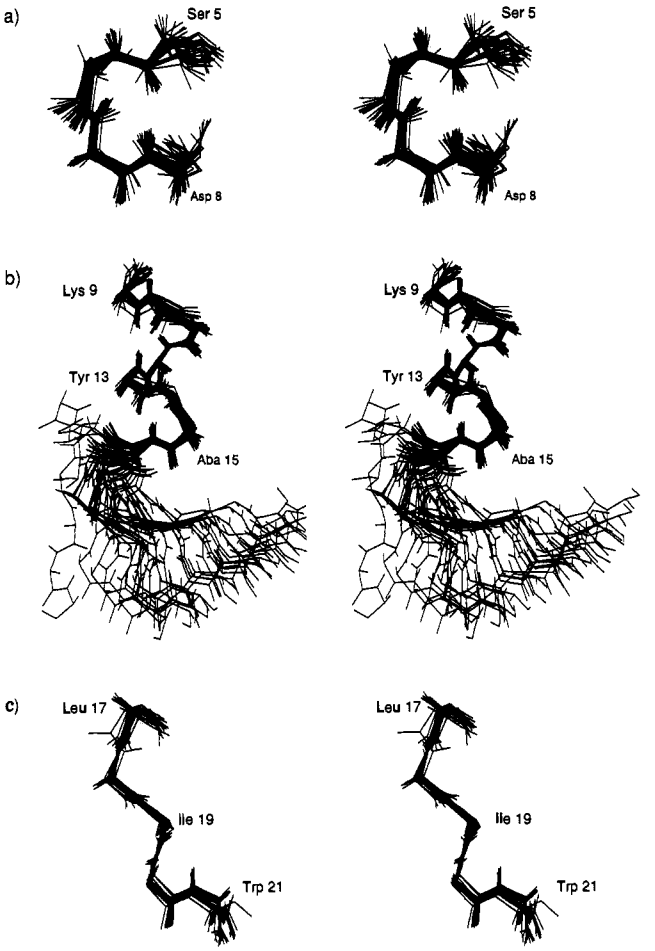

Figure 7. Stereoviews of 30 calculated structures for [1,15 Aba]-ET-1 superimposed on the basis of back-bone atoms: (a) β-turn region from residues 5 to 8, (b) helical region from residues 9 to 16, and (c) C-terminal region from residues 17 to 21. Also shown in (b) but not included in the superimposition are the C-terminal region residues 17–21. The range of conformational space occupied by the C-terminal region relative to the helix is demonstrated. A good superimposition (rmsd = 0.42 Å) is obtained within the C-terminal region, as shown in (c).

by a hydrogen bond between Asp8 HN and Ser5 CO. In most structures, an additional hydrogen bond is formed between Met7 HN and Ser5 CO. The involvement of Asp8 HN in a hydrogen bond is supported by its slow exchange with D_2O solvent; however, as both Met7 HN and Met7 Hα are unresolved, the involvement of Met7 HN in a hydrogen bond could not be confirmed. Standard torsion angles for a type I β-turn[23] are shown in Table 2 for comparison with the derived angles. For the central residues (i.e., 6 and 7) of the proposed β-turn, there is a close match of the experimentally determined angles to those expected for a standard type I turn. The set of 30 accepted structures shows no deviations greater than 0.3 Å from the NOE constraints over this segment and no deviations from the dihedral constraints. A superimposition of this set on the basis of back-bone atoms is shown in Figure 7a. The rmsd of this superimposition, calculated as the average of all possible pairwise comparisons, is 0.60 Å.

Helix. The pairwise rms deviation of the superimposition over the helical region from residues 9 to 16 is 0.52 Å. Analysis of the calculated structures for the deviation of distance and dihedral constraints revealed that several constraints, mostly of the type $d_{\alpha N}(i, i+1)$ and $d_{\beta N}(i, i+1)$, are violated, albeit to a small degree (<0.3 Å), in most

of the structures in the helical segment (residues 9–16). While NOE connectivities observed in this segment are consistent with the helical structure (i.e., $d_{NN}(i, i+1)$, $d_{\alpha N}(i, i+3)$, and $d_{\alpha\beta}(i, i+3)$, etc.), the intensity of some connectivities, particularly the strong $H_{\alpha i}$–H_{Ni+1}, is more consistent with an extended structure. $^3J_{HN\text{-}H\alpha}$ coupling constants in this segment are also larger than expected for residues in an α-helix. These observations are in keeping with some degree of motional averaging between an α-helical and a more extended structure. The calculated structure must therefore be viewed as an approximate time average of two or more contributing structures. Also, the pattern of H-bonds observed is not that of a regular α-helix; two 3 → 1 H-bonds, more characteristic of a 3–10 helix, are observed (Val12 HN → Lys9 CO and Aba15 HN → Val12 CO). The average torsion angles given in Table 2 show that most residues differ considerably from standard helical values ($\phi = -60°$, $\psi = -60°$). The deviation from helical torsion angles results in an opening of the helix so that the Phe14 HN → Glu10 CO hydrogen bond is not formed. This observation is consistent with the observation of a strong NOE connectivity between Val12 Hα and Tyr13 HN.

C-Terminus. A qualitative analysis of the experimental data, particularly the dense network of NOE connectivities and the slow exchange of the amide protons of Ile19 and Ile20, provides evidence for the presence of well-defined structural elements in the C-terminal segment. However, a number of NOE constraints involving the Ile19 γ-methyl group and the Ile19 HN–Ile20 HN constraint were violated in most structures. Preliminary calculations also failed to suggest possible acceptors for the slowly exchanging amide protons of residues 19 and 20. These observations probably result from the high degree of motional averaging for the region. Under these conditions, no single structure is consistent with all the experimental data and the structure determined must be considered as an approximate time average.

Figure 7b shows the relative spread of orientations of the C-terminus relative to the helical region. While the C-terminal region occupies a large region of conformational space, within itself it exists primarily as an extended structure. This is illustrated in Figure 7c, which shows a superimposition of the C-terminus for 30 calculated structures. The rmsd of the superimposition is 0.42 Å.

N-Terminus. The N-terminal region (residues 1–4) of the calculated structures shows no preferred conformation, as demonstrated by the generally low angular order parameters for torsion angles in this region (see Figure 6). The predicted lack of structure in the segment is supported by the lower than expected intensity of some NOESY cross peaks. In particular, there is an absence of $d_{NN}(i, i+1)$ connectivities for residues 2 and 3. In addition to the lack of a well-defined local geometry, the orientation of the N-terminal segment relative to the remainder of the peptide also varies considerably. This variation results in a wide range of displacements of Aba1 with respect to Aba15 and, in particular, a wider range than would be expected for native ET-1 where residues 1 and 15 are involved in a disulfide bridge. This is illustrated in Figure 8, where the positions of Aba1 N in the calculated structures are indicated on a superimposition of the helical segment.

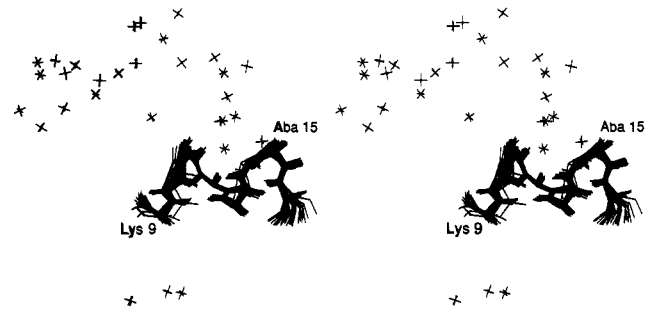

Figure 8. Stereoview of 30 calculated structures for [1,15 Aba]-ET-1 over the back-bone atoms for the helical region, residues 9–16. The range of positions for the N-terminal charge (Aba1 N), indicated with a cross, is much higher than would be expected for native ET-1 where residues 1 and 15 are linked by a disulfide bridge.

Discussion

One difficulty in comparing the solution structures of [1,15 Aba]-ET-1 with those of native ET-1 is the range of differing structures for ET-1 and related peptides previously reported in the literature. Despite the general similarity of all structures reported for peptides of the endothelin family, including ET-3 and sarafotoxin 6b, significant differences occur in specific structural details. These differences include the number of amino acid residues involved in the helix, the nature of this helix, the presence or absence of a turn at residues 5–8, and the conformation and degree of disorder reported for the C-terminus (see Table 3). Mills et al.[35] concluded that most of the discrepancies are more than likely due to either the nature of the solvents used in the previous studies or the methods used for deriving refined structures from the NMR data. Any comparison between the [1,15 Aba]-ET-1 analogue and ET-1 must therefore take differences in solution conditions into account. In view of this, the following discussion comparing solution structures is aimed

Table 3. Summary of the Solution Conformations of the Endothelin Peptides Defined from Previous NMR Studies

peptide	helical region	turn	C-terminal	solvent	reference
ET-1	K9–C15	structured (not defined)	undefined	DMSO	24
ET-1	undefined	undefined	associated with bicyclic core	DMSO	25
ET-1	L6–C15[a]	undefined[a]	undefined	DMSO	26
ET-1	K9–C15	undefined	undefined	30% CDCN/H_2O	27
ET-1	K9–L17	S5–D8	structured (undefined)	60% ethylene glycol/H_2O (with TFA)	28
ET-1	K9–F14	averaging (reverse turn, S5–D8)	averaging	60% ethylene glycol/H_2O (with TFA)	29
ET-1	K9–C15	S5–D8 (β-bend)	undefined	10% acetic acid/H_2O	30
ET-1	K9–H16	S5–D8 (β-bend)	extended	40% acetic acid/H_2O	31
[Nle^7]-ET-1	K9–H16	S5–D8 (quasi-turn)	extended	DMSO and also 50% CDCN/H_2O	32
ET-3	K9–C15		apposed to bicyclic core	H_2O	33
ET-3	K9–C15	undefined	apposed to bicyclic core	10% acetic acid/H_2O	34
sarafotoxin 6b	K9–L17	undefined	undefined	H_2O	35

[a] Reevaluation of the original data revealed that it would be equally possible to describe residues 9–15 as helical, with 6–8 involved in a β-turn or a "loose" helical turn.

at identifying differences that are significant relative to the range of conformations available for ET-1.

The helical region spanning segments of the bicyclic core is a common structural feature of all the endothelin peptides studied to date. The helix is also observed (between residues Lys9 and His16) in the conformation of [1,15 Aba]-ET-1 derived in this study. The slightly irregular nature of the helix observed for the monocyclic ET-1 analogue, particularly the absence of a 14–10 hydrogen bond and the presence of a shorter 12–9 hydrogen bond, was also noted in ET-1 by Andersen et al.[29] It can therefore be concluded that there is no significant difference in the solution structures of [1,15 Aba]-ET-1 and ET-1 through this helical region, despite the absence of the disulfide linkage between residues 1 and 15 in the analogue.

A second structural feature of the endothelin peptides is the proposed turn around Ser5–Asp8 which has been variously reported in previous NMR studies (Table 3). Krystek et al.[28] and Andersen et al.[29] reported that the conformation around Ser5–Asp8 in ET-1 was averaging and that no well-defined geometry consistent with a definitive type of β-turn could be identified. A planar quasi-turn conformation between residues 4 and 9 was noted by Aumelas[32] for the [Nle7]-ET-1 analogue, and both Tamaoki et al.[30] and Dalgarno et al.[31] reported a type I β-turn around Ser5–Asp8 in ET-1. A well-defined type I β-turn is observed for the [1,15 Aba]-ET-1 analogue in the current study, indicating that there is no significant difference in the solution conformation for ET-1 and the monocyclic analogue in this region of the peptide sequence.

The C-terminus of the endothelin peptides is particularly interesting due to the differences in conformation reported for the terminal hexapeptides in ET-1 and ET-3 in various solvent mixtures, despite the fact that this region is completely conserved in both peptides. Mills et al.[33] and Bortmann[34] both reported that the C-terminus of ET-3 folds back to interact with the bicyclic core. Similarly, Saudek et al.[25] reported that the tail region of ET-1 in DMSO interacts with the bicyclic core. However, none of the other studies of ET-1 in various solvents (Table 3) detected such an interaction. Most studies reported that the conformation of the C-terminal region of ET-1 was undefined. The current study has shown that there is some degree of structuring in the C-terminal hexapeptide of the [1,15 Aba]-ET-1 fragment, although a single conformation consistent with all the experimental data could not be derived. This has also been noted for ET-1 by Krystek et al.[28] and Andersen et al.,[29] with both studies concluding that high degrees of motional averaging occur in this region and that no defined secondary structure was present.

The unusually high-field chemical shift of the γ-methyl for Ile19, which has been reported in most NMR studies of the endothelin peptides (e.g., Andersen et al.,[29] Mills et al.,[33] and Dalgarno et al.[31]), is also observed for the [1,15 Aba]-ET-1 analogue. This suggests that although the conformation of the tail in the endothelins is averaging, the electronic environments experienced by Ile19 in each peptide are similar. Again, it must be concluded that there are no significant differences in the solution conformation of ET-1 and [1,15 Aba]-ET-1 around the C-terminus of these two peptides.

The only region of the endothelin peptides that remains to be compared to the monocyclic analogue is the N-terminus. Almost without exception, previous NMR studies have identified this as the least-structured region of the endothelin peptides. This is also seen in the [1,15 Aba]-ET-1 analogue, which is not surprising as the conformational restraint of the disulfide bridge between Cys1–Cys15 in ET-1 has been removed. On the basis of the geometric spread of the calculated structures, the degree of conformational variability appears to be greater in the monocyclic analogue than in ET-1.

From the discussion above, it can be concluded that the solution conformations of ET-1 and [1,15 Aba]-ET-1 are generally similar. This is consistent with the observation that CD spectra of endothelin and the monocyclic analogues [1,15 Ala]-ET-1 and [3,11 Ala]-ET-1 are qualitatively similar.[36] Interestingly, the CD study[36] also predicted that the three peptides had a β-turn involving residues Asp8–Cys11 and a β-sheet region extending from Val12 to Trp21, secondary structure which is inconsistent with all the NMR solution structures reported so far.

The similarity in the derived solution conformations of ET-1 and the [1,15 Aba]-ET-1 analogue is interesting, given the different pharmacological profiles of a range of related peptides at ET_A and ET_B receptors. ET-1, ET-2, ET-3, and several linear analogues are potent agonists at the ET_B receptor, many showing marked selectivity for ET_B compared with ET_A.[12,17] By contrast, there is a larger range in potency at the ET_A receptor,[12] with a marked decrease in activity as the disulfide linkages in the peptides are excluded.[14] The difference in activity profiles for this group of peptides at the two endothelin receptor sites needs to be considered when comparing conformational data with pharmacological activity.

Several residues of ET-1 have been identified as being important for ET_A agonism, including Asp8, Glu10, Phe14, His16, Leu17, Asp18, and Trp21.[15,37] All of these residues are in regions of the sequence where the conformation is conserved in the monocyclic analogue studied here. This suggests that conformational differences in other regions of the molecule are responsible for differences in activity of bicyclic and monocyclic analogues at the ET_A receptor. Most of the amino acid differences between ET-1, ET-2, and ET-3 occur within residues 2–7. Replacement of the 1–15 disulfide bond in ET-1 with an amide linkage results in what appears to be an ET_A antagonist,[38] while N-acetylation of ET-1 dramatically reduces the agonist activity of ET-1 at the ET_A receptors.[15] This implies that differences in pharmacological activity profiles for the endothelins and their analogues at ET_A receptors are at least partially due to the conformation of residues 1–3 (and hence the position of the N-terminal charge) relative to the rest of the molecule, as well as to the nature of the amino acids in positions 2–7. This is supported by our study, which finds that the solution conformation for residues 6–21 is the same in ET-1 and the [1,15 Ala]-ET-1 analogue, but is different for residues 1-3. As side-chain orientations are not fully defined in the various solution structures of the endothelins, the possibility also exists of differences in activity reflecting different side-chain orientations, even though the global fold is similar.

Activity at the ET_B receptors is similar for all three endothelin isopeptides and the analogues 4-Ala-ET-1, 4-Ala-ET-1 (6–21), N-Ac-4-Ala-ET-1, and N-Ac[11,15-Ala]-ET-1 (6–21)[12,17] (known as BQ3020). The [3,11 Ala]-ET-1 analogue is approximately 1 order of magnitude less potent[16] than these peptides and the [1,15 Ala]-ET-1

analogue approximately 2 orders less potent, indicating that, as is the case for the ET_A receptor, the "outside" disulfide link is more important than the internal disulfide link in maintaining the activity of monocyclic analogues. Removal of both disulfides, however, results in a linear ET-1 analogue (4-Ala-ET-1) equipotent with ET-1 in binding at the ET_B receptor.[12] Also, substitution of amino acids in positions 2–7 (where most of the differences between ET-1 and ET-3 occur), or even removal of residues 1–5 (i.e., in 4-Ala-ET-1 (6–21) and BQ3020), does not significantly change the affinity of these peptides at the ET_B site. Such a structure–activity profile for binding implies that neither the topography of residues in positions 1–3 nor the nature of amino acids in the region 2–7 is important for agonist activity at the ET_B receptor. This is in contrast to the interactions at the ET_A receptor, where the orientation of the N-terminal charge relative to the rest of the molecule appears to be important.

Conclusions

The solution conformation of [1,15 Aba]-ET-1 comprises a type I β-turn through residues 5–8, a helical region for residues 9–15, and a structured but ill-defined C-terminal region encompassing residues 16–21. The N-terminus contains neither a recognized structural motif nor a definitive orientation relative to the rest of the peptide. This solution conformation is similar to those previously reported for ET-1. It appears likely that increased structural disorder at the N-terminus produces a decrease in activity at ET_A receptors but has little effect at ET_B receptors.

Experimental Section

NMR Spectroscopy. [1,15 Aba]-ET-1 was obtained from Auspep Pty. Ltd. and used without further purification. Experience with members of the endothelin family has shown that these peptides exhibit poor aqueous solubility and are subject to aggregation phenomena.[39] [1,15 Aba]-ET-1 likewise proved difficult to dissolve in aqueous media, and some experimentation was necessary to find a suitable solvent system. The solvent system found to give the best results was an aqueous solution containing 10% acetonitrile and 1.5% acetic acid. Samples of 1.5–3.0 mg of peptide were first dissolved in 60 μL of acetonitrile-d_3 containing 9 μL of acetic acid-d_4, and then diluted to a sample volume of 600 μL with H_2O or D_2O to give a final sample concentration of 1–2 mM at pH = 3.3. Samples were then transferred to 5-mm NMR tubes (Wilmad Glass Co. 535 PP) for immediate use. Samples prepared in this manner have a useful lifetime of approximately 1 week, after which aggregation of the peptide led to broadening of NMR resonances. Following aggregation, the peptide was not recoverable.

NMR spectra were obtained at 600 MHz on a Bruker AMX 600 spectrometer over a spectral width of 6096 Hz using the phase-sensitive TPPI method of acquisition for all 2D experiments. For NOESY spectra[40] in protic media, suppression of the water signal was achieved using a jump-return selective excitation sequence to create an excitation null at the carrier frequency.[41] Signal suppression obtained by this means was supplemented by low-power irradiation during the relaxation delay and mixing time. For other experiments, water suppression was achieved by continuous irradiation during the relaxation delay and, in the case of NOESY spectra in D_2O, during the mixing time.

Four NOESY spectra were acquired, each with a mixing time of 200 ms, under the following conditions: H_2O 298 K, H_2O 293 K, D_2O 293 K, and H_2O 288 K. Each experiment consisted of 256–512 t_1 increments with 2048 complex data points in F_2. Data was apodized using a 90°-shifted sine-bell-squared window function before zero filling, yielding 1K × 1K real data matrices. Base-line correction was performed separately on each side of the residual water signal.

DQF-COSY[42] and TOCSY[43] spectra were acquired at 298 K with 512 and 256 t_1 increments, respectively, and 2048 complex data points in F_2. Apodization was performed typically with a 60°-shifted sine-bell window function, and data sets were zero filled to 2K × 2K real matrices.

All processing was performed on a Silicon Graphics IRIS 4D/30 workstation using standard Bruker software (UXNMR) for NOESY spectra and FELIX[44] (Hare Research) for DQF-COSY and TOCSY spectra.

Measurement of Cross-Peak Volumes. The intensity of all well-resolved cross peaks in the 200-ms NOESY spectra in H_2O and D_2O was measured by volume integration. In addition, the heights of these cross peaks were measured by counting peak contour levels to establish calibration curves for cross-peak height versus volume. One calibration curve was constructed for each resonance under the assumption that all cross peaks of a particular resonance have the same cross-peak height versus volume ratio. Contour levels measured for overlapped peaks were then converted into volume estimates. Diagonal peaks were classed as follows: amide, α, methylene, methine, aromatic, and all other protons. As many well-resolved diagonal intensities as possible were measured for each class, with unquantifiable diagonals represented by class averages. Peak volumes measured from the experiment in D_2O were then scaled such that a selection of well-resolved diagonal and cross peaks were of equal intensity to those in the H_2O experiment. This combined set of peak volumes was then used to estimate interproton distances.

Extraction of Distance Constraints. Diagonal and cross-peak volumes were converted into distance estimates using the full-relaxation matrix program DISCON.[45] Input parameters for DISCON and associated programs include experimental conditions (NOESY mixing time, relaxation delay, and spectrometer field, etc.) and a functional molecular correlation time (τ_c). The latter is estimated from the best fit of simulated spectra to experimental data, i.e., cross-peak to diagonal volume ratios for protons whose separation is known. This procedure gave an effective τ_c of 2 ns at 293 K. A fully extended linear chain, i.e., without the disulfide bridge, was used as the starting structure for the iterative calculation of distance constraints. A first generation of distance constraints was derived from this structure. Structures resulting from simulated annealing calculations using the first-generation distance constraints were used as the input to further rounds of DISCON, which in turn produced second-generation distance constraints. This procedure was repeated to generate a third generation of distance constraints which were used for the final structure calculations.

Interproton distances were converted into constraints with a tolerance of ±20%. For methylene, aromatic, and leucine methyl resonances which could not be assigned stereospecifically, the DISCON calculated distances were converted into upper distance constraints by the addition of appropriate pseudoatom allowances.[20] A similar procedure was applied for the methyl resonances of Ile20, which are of equivalent chemical shift. Some resonances were well resolved at 288 K only, but as the lower temperature implies a different correlation time, intensities drawn from a NOESY spectrum at this temperature were not included in the DISCON analysis. Rather, these intensities were applied as upper distance constraints, based on their classification as strong, medium, weak, or very weak (2.7, 3.2, 4.0, and 5.0 Å, respectively).

Torsion Angle and H-Bond Constraints. The possible ranges of back-bone torsion angles were obtained from $^3J_{HN\text{-}H\alpha}$ coupling constants. Where possible, these were measured for amide-proton peaks in 1D spectra. In cases of overlap, coupling constants were measured from F_2 slices extracted from the DQF-COSY spectrum in H_2O, where they were inverse-Fourier-transformed and zero-filled to a resolution of 0.75 Hz/point. Coupling constant values were measured together with half-height line widths and deconvoluted to remove distortions due to overlap of the antiphase peak components. Coupling constants of less than 6.0 Hz or greater than 8.0 Hz were considered significant for use as constraints in structure calculations (−60° ± 30° and −120° ± 50°, respectively).[20,46]

The possible involvement of amide protons in hydrogen bonds was investigated by measuring their rate of exchange with solvent. Proton resonances still visible in 1D spectra 40 min after dissolution of the peptide in deuterated solvent were considered to be slowly exchanging. Some of these resonances were overlapped, and because of the time needed to prepare samples and the low concentration of the sample solution, 2D spectra could not be obtained to resolve ambiguous assignments. However, assignments were made on the basis of differences in α-proton peaks in partly exchanged and fully exchanged 1D spectra (i.e., 40 and 150 min after addition of D_2O). Coupling of the α-proton to the slowly exchanging amide protons broadened and lowered the intensity of the α-proton signals in the partly exchanged spectrum. Amide protons identified as slowly exchanging were considered for use as hydrogen-bond constraints in structure calculations. These constraints were applied as pseudo-NOE distances of *HN*–*CO* = 1.58–2.30 Å and H*N*–*CO* = 1.58–3.20 Å.

Simulated Annealing Calculations. To determine the 3D structure of [1,15 Aba]-ET-1, the experimental data were included in *in vacuo* simulated annealing calculations using XPLOR 3.0[53] on a Silicon Graphics IRIS 4D/30 workstation. Starting structures for the simulation were generated by subjecting a structure created by randomizing atom coordinates to a combination of dynamics and energy minimization. This yielded a "template" with essentially random torsion angles but with correct covalent geometry and low nonbonded energy. The standard XPLOR forcefield parameter set for simulated annealing (PARALLHDG.PRO) was used to create sets of 40 structures using a standard protocol.[47] In this protocol, nonbonded interactions were modeled with the purely repulsive "repel" function, i.e., electrostatic terms are ignored. The S–S bond forming the disulfide bridge was initially disconnected and replaced with a pseudo-NOE constraint during the high-temperature dynamics to allow a more thorough search of conformational space and then formally bonded before commencement of the cooling stage.

Structures calculated by the simulated annealing protocol were refined by an additional stage of simulated annealing and minimization.[47] This refinement procedure used higher weighting on experimental constraints, via the use of the square potential well for the NOE energy term and increased dihedral constraint scale factor, to produce structures with lower constraint violations. Finally, the structures were relaxed via minimization to a gradient of 0.01 in a slightly modified version of the more complete PARMALLH3X.PRO force-field parameter set. This parameter set was modified so that 1–4 nonbonded interactions were calculated explicitly, i.e., force constants on dihedrals around rotatable bonds were set to zero and 1–4 interactions were included in the calculations by setting NBXMOD = 3.[47] Experimental constraints were included during the minimization using scale factors of 10 and 5 for NOE and dihedral constraints, respectively.

Acknowledgment. This work was supported in part by a grant from the Australian Research Council. We thank Dr. Denis Scanlon and Dr. Stephen Kent for helpful discussions during the design of this peptide. We also thank Jacqui King for her excellent work in preparing the manuscript.

References

(1) Yanagisawa, M.; Kurihara, H.; Kimura, S.; Tomobe, Y.; Kobayashi, M.; Mitsui, Y.; Yazaki, Y.; Goto, K.; Masaki, T. A Novel Potent Vasoconstrictor Peptide produced by Vascular Endothelial Cells *Nature* **1988**, *332*, 411–415.

(2) Inoue, A.; Yanagisawa, M.; Kimura, S.; Kasuya, Y.; Miyuachi, T.; Goto, K.; Masaki, T. The Human Endothelin Family: Three Structurally and Pharmacologically Distinct Isopeptides predicted by Three Separate Genes. *Proc. Natl. Acad. Sci. U.S.A.* **1989**, *86*, 2863–2867.

(3) Itoh, Y.; Kimura, C.; Ona, H.; Fujino, M. Canine Endothelin-2: cDNA Sequence for the Mature Peptide. *Nucleic Acids Res.* **1989**, *17*, 5389.

(4) Kimura, C.; Itoh, Y.; Okhubo, S.; Ogi, K.; Onda, H.; Funino, M. Cloning and Sequencing of a Canine Gene Segment encoding Mature Endothelin. *Nucleic Acids Res.* **1989**, *17*, 3290.

(5) Yanagisawa, M.; Inoue, A.; Ishikawa, T.; Kasuya, Y.; Kimura, S.; Kumagaye, S.; Nakajima, K.; Watanabe, T. X.; Sakakibara, S.; Goto, K.; Masaki, T. Primary Structure, Synthesis and Biological Activity of Rat Endothelin, an Endothelium-Derived Vasoconstrictor Peptide. *Proc. Natal. Acad. Sci. U.S.A.* **1988**, *85*, 6964–6967.

(6) Okhubo, S.; Itoh, Y.; Kimura, C.; Ondsa, H.; Fujino, M. Nucleotide Sequence of a Rabbit Genomic DNA encoding Mature Endothelin-3. *Nucleic Acids Res.* **1990**, *18*, 374.

(7) Saida, K.; Mitsui, Y.; Ishida, N. A Novel Peptide, Vasoactive Intestinal Contractor, of a New (Endothelin) Peptide Family. *J. Biol. Chem.* **1989**, *264*, 14613–14616.

(8) Kloog, Y.; Ambar, I.; Sokolovsky, M.; Kochva, E.; Wollberg, Z.; Bdolah, A. Sarafotoxin, a Novel Vasoconstrictor Peptide: Phosphoinositide Hydrolysis in Rat Heart and Brain. *Science* **1988**, *242*, 268–270.

(9) Arai, H.; Hori, S.; Aramori, I.; Okhubo, H.; Nakanishi, S. Cloning and Expression of a cDNA encoding an Endothelin Receptor. *Nature* **1990**, *348*, 730–732.

(10) Sakurai, T.; Yanagisawa, M.; Takuwa, Y.; Miyazaki, H.; Kimura, S.; Goto, K.; Masaki, T. Cloning of a cDNA encoding a Non-isopeptide-Selective Subtype of the Endothelin Receptor. *Nature* **1990**, *348*, 732–735.

(11) Maggi, C. A.; Giuliani, S.; Ptacchini, R.; Rover, P.; Giachetti, A.; Meli, A. The Activity of Peptides of the Endothelin Family in Various Mammalian Smooth Muscle Preparations. *Eur. J. Pharmacol.* **1989**, *174*, 23–31.

(12) Saeki, T.; Ihara, M.; Fukuroda, T.; Yamagiwa, M.; Yano, M. [Ala1,3,-11,15]-Endothelin-1 Analogs with ET_B Agonistic Activity. *Biochem. Biophys. Res. Commun.* **1991**, *179*, 286–292.

(13) Miller, R. C.; Pelton, J. T.; Huggins, J. P. Endothelins - from Receptors to Medicine. *Trends Pharmacol. Sci.* **1993**, *14*, 54–60.

(14) Sokolovsky, M.; Structure-Function Relationships of Endothelins, Sarafotoxins, and their Receptor Subtypes. *J. Neurochem.* **1992**, *59*, 809-821.

(15) Nakajima, K.; Kubo, S.; Kumagaye, S.; Nishio, H.; Tsunmi, M.; Inui, T.; Kuroda, H.; Chino, N.; Watanabe, T. X.; Kimura, T.; Sakakibara, S. Structure-Activity Relationships of Endothelin: Importance of Charged Groups. *Biochem. Biophys. Res. Commun.* **1989**, *163*, 424–429.

(16) Hiley, R. C.; Jones, C. R.; Pelton, J. T.; Miller, R. C. Binding of [^{125}I]-Endothelin-1 to Rat Cerebellar Homogenates and its Interactions with Some Analogues. *Br. J. Pharmacol.* **1990**, *101*, 319–324.

(17) Ihara, M.; Saeki, T.; Fukuroda, T.; Kimura, S.; Ozaki, S.; Patel, A. C.; Yano, M. A Novel Radioligand [^{125}I]BQ-3020 Selective for Endothelin (ET_B) Receptors. *Life Sci.* **1992**, *51*, PL 47–52.

(18) Cody, W. L.; Doherty, A. M.; XiaQiang, He.; Rapundalo, S. T.; Hingorani, G. P.; Panek, R. L.; Major, T. C. Monocyclic Endothelins: Examination of the Importance of the Individual Disulfide Rings. *J. Cardiovasc. Pharmacol.* **1991**, *17*(S7), S62–S64.

(19) Wlodawer, A.; Miller, M.; Jaskolski, M.; Sathyanarayana, B. K.; Baldwin, E.; Weber, I. T.; Selk, L. M.; Clawson, L.; Schneider, J.; Kent, S. B. H. Conserved Folding in Retroviral Proteases: Crystal Structure of a Synthetic HIV-1 Protease. *Science* **1989**, *245*, 616–621.

(20) Wûthrich, K. *NMR of Proteins and Nucleic Acids*; John Wiley: New York, 1986.

(21) Driscoll, P. C.; Clore, G. M.; Beress, L.; Gronenborn, A. M. A Proton Nuclear Magnetic Resonance Study of the Antihypertensive and Antiviral Protein BDS-1 from the Sea Anenome *Anemonia sulcata*: Sequential and Stereospecific Resonance Assignment and Secondary Structure. *Biochemistry* **1989**, *28*, 2178–2187.

(22) Detlefsen, D. J.; Thanabal, V.; Pecoraro, V. L.; Wagner, G. Solution Structure of Fe(II) Cytochrome c551 from *Pseudomonas aeruginosa* as determined by Two-Dimensional ^{1}H NMR Spectroscopy. *Biochemistry* **1991**, *30*, 9040–9046.

(23) Rose, G. D.; Gierasch, L. M.; Smith, J. A. Turns in Peptides and Proteins. *Adv. Protein Chem.* **1985**, *37*, 1–107.

(24) Endo, S.; Inooka, H.; Ishibashi, Y.; Kitada, C.; Mizuta, O.; Fujino, M. Solution Conformation of Endothelin determined by Nuclear Magnetic Resonance and Distance Geometry. *FEBS Lett.* **1989**, *257*, 149–154.

(25) Saudek, V.; Hoflack, J.; Pelton, J. T. ^{1}H NMR Study of Endothelin, Sequence-Specific Assignment of the Spectrum and a Solution Structure. *FEBS Lett.* **1989**, *257*, 145–148.

(26) Munro, S. L.; Craik, D. J.; McConville, D.; Hall, J. G.; Searle, M.; Bicknell, W.; Scanlon, D.; Chandler, C. Solution Conformation of Endothelin, a Potent Vasoconstricting Bicyclic Peptide. A Combined Use of ^{1}H NMR Spectroscopy and Distance Geometry Calcualtions. *FEBS Lett.* **1991**, *278*, 9–13.

(27) Reily, M. D.; Dunbar, J. B., Jr. The Conformation of Endothelin-1 in Aqueous Solution: NMR-Derived Constraints combined with Distance Geometry and Molecular Dynamics Calculations. *Biochem. Biophys. Res. Commun.* **1991**, *178*, 570–577.

(28) Krystek, S. R.; Bassolino, D. A.; Novotny, J.; Chen, C.; Marschner, T. M.; Andersen, N. H. Conformation of Endothelin in Aqueous Ethylene Glycol determined by ^{1}H NMR and Molecular Dynamics Simulations. *FEBS Lett.* **1991**, *281*, 212–218.
(29) Andersen, N. H.; Chen, C.; Marschner, T. M.; Krystek, S. R., Jr.; Bassolino, D. Conformtional Isomerism of Endothelin in Acetic Acid Media: a Quantitative NOESY Analysis. *Biochemistry* **1992**, *31*, 1280–1295.
(30) Tamaoki, H.; Kobayashi, Y.; Nishimura, S.; Ohkubo, T.; Kyoguku, Y.; Nakajima, K.; Kumagaye, S.; Kimura, T.; Sakakibara, S. Solution Conformation of Endothelin determined by Means of ^{1}H NMR Spectroscopy and Distance Geometry Calculations. *Protein Eng.* **1991**, *4*, 509–518.
(31) Dalgarno, D. C.; Slater, L.; Chackalamannil, S.; Senior, M. M. Solution Conformation of Endothelin and Point Mutants by Nuclear Magnetic Resonance Spectroscopy. *Int. J. Peptide Protein Res.* **1992**, *40*, 515–523.
(32) Aumelas, A.; Chiche, L.; Mahe, E.; L-Nguyen, D.; Sizun, P.; Berthault, P.; Perly, B. Determination of the Structure of [Nle^7]-Endothelin by ^{1}H NMR. *Int. J. Peptide Protein Res.* **1991**, *37*, 315–324.
(33) Mills, R. G.; O'Donoghue, S. I.; Smith, R.; King, G. F. Solution Structure of Endothelin-3 determined using NMR Spectroscopy. *Biochemistry* **1992**, *31*, 5640–5645.
(34) Bortmann, P.; Hoflack, J.; Pelton, J. T.; Saudek, V. Solution Conformation of Endothelin-3 by ^{1}H NMR and Distance Geometry Calculations. *Neurochem. Int.* **1991**, *18*, 491–496.
(35) Mills, R. G.; Atkins, A. R.; Harvey, T.; Junius, F. K.; Smith, R.; King, G. F. Conformation of Sarafotoxin 6b in Aqueous Solution determined by NMR Spectroscopy and Distance Geometry. *FEBS Lett.* **1991**, *2*, 247–252.
(36) Pelton, J. T.; Miller, R. C. The Role of the Disulphide Bonds in Endothelin-1. *J. Pharm. Pharmacol.* **1991**, *43*, 43–45.
(37) Watanabe, T. X.; Itahara, Y.; Nakajimi, K.; Kumagaye, S.; Kimura, T.; Sakakibara, S. The Biological Activity of Endothelin-1 Analogues in Three Different Assay Systems. *J. Cardiovasc. Pharmacol.* **1991**, *17*(7), S5–S9.
(38) Spinella, M. J.; Malik, A. B.; Everitt, J.; Andersen, T. T. Design and Synthesis of a Specific Endothelin 1 Antagonist: Effects on Pulmonary Vasoconstriction. *Proc. Natl. Acad. Sci. U.S.A.* **1991**, *88*, 7443–7446.
(39) Bennes, R.; Calas, B.; Chabrier, P.-E.; Demaille, J.; Heitz, F. Evidence for Aggregation of Endothelin 1 in Water. *FEBS Lett.* **1990**, *276*, 21–24.
(40) Macura, S.; Ernst, R. R. Elucidation of Cross-Relaxation in Liquids by Two-Dimensional NMR Spectroscopy. *Mol. Phys.* **1980**, *41*, 91–117.
(41) Plateau, P.; Gueron, M. Exchangeable Proton NMR without Baseline Distortion using New Strong-Pulse Sequences. *J. Am. Chem. Soc.* **1982**, *104*, 7310–7311.
(42) Rance, M.; Sørensen, O. W.; Bodenhausen, G.; Wagner, G.; Ernst, R. R.; Wüthrich, K. Improved Spectral Resolution in ^{1}H NMR Spectra of Proteins via Double Quantum Filtering. *Biochem. Biophys. Res. Commun.* **1983**, *117*, 479–485.
(43) Braunschweiler, L.; Ernst, R. R. Coherence Transfer by Isotropic Mixing: Application to Proton Correlation Spectroscopy. *Mol. Phys.* **1983**, *53*, 521–528.
(44) Hare Research Inc., 18943 120th Avenue NE, Suite 104, Bothell, WA 98011.
(45) Andersen, N. H.; Lai, X.; Marschner, T. *NOESYSIM/DISCON Documentation*; University of Washington: Seattle, WA, 1990.
(46) Pardi, A.; Billeter, M.; Wüthrich, K. Calibration of the Angular Dependence of the Amide Proton-Cα Proton Coupling Constants, $^3J_{NH\alpha}$ in a Globular Protein. *J. Mol. Biol.* **1984**, *180*, 741–751.
(47) Brünger, A. T. *XPLOR Manual*; Yale University: New Haven, CT, 1990.